Experimental studies of shear bands in Zr-Cu metallic glass

V. Nekouie[a], S. Doak[c], A. Roy[a*], U. Kühn[b], V. V. Silberschmidt[a]

[a] Wolfson School of Mechanical, Electrical and Manufacturing Engineering, Loughborough University, Leicestershire, UK

[b] Leibniz IFW Dresden, Institute for Complex Materials, Helmholtzstraße 20, D-01069 Dresden, Germany

[c] Loughborough Materials Characterisation Centre, Department of Materials, Loughborough University, Leicestershire, UK

*Corresponding author's e-mail: A.Roy3@lboro.ac.uk

Abstract. Shear bands are the key feature that controls deformation in bulk metallic glasses (BMGs). This study provides a comprehensive analysis of plastic deformation of a Zr-Cu-based BMG at room temperature. Experiments were conducted to observe the evolution of shear bands in the material. It was shown that shear bands formed discretely in the material which allows for material deformation to occur across it. Additionally, individual shear bands were characterised to obtain a better understanding of shear-band-induced plasticity. Assessment of mechanical properties, such as hardness and elastic modulus, indicate the deformed regions of the material were weaker than undeformed regions. No compositional or structural changes were found in shear-band of the studied BMG suggesting generation of local free volume in the deformed region.

Keywords: Metallic glass, Shear bands, Indentation, Plastic deformation

1 Introduction

Bulk metallic glasses (BMGs) have attracted considerable attraction as structural materials due to their high strength and superior elasticity [1-6]. At room temperature, inelastic deformation behaviour in BMGs are strongly governed by the formation of shear bands (SBs), making an investigation of their origin, evolution and properties a pre-condition for interpretation of mechanisms of plastic deformation of BMGs [7,8]. Several studies were recently carried out, for example, on propagation dynamics of an individual shear band

(SB) and interactions between them [9,10], effects of extrinsic factors including sample size, machine stiffness, testing temperature and strain rate on shear-banding behaviour [11-14] and *in-situ* or quasi-*in situ* observations of SB evolution [15-17].

Localisation of shear deformation induces intense strain softening in BMGs; mechanism for which are debated [18]. Deformation-induced nanocrystallisation was observed in some BMGs under large plastic deformation [7,11,19], under compression [20], nanoindentation [21] and ball-milling processes [14]. It was suggested that *in-situ* nanocrystallisation within SBs resulted in the bifurcation of their propagation, indicating branching and healing mechanisms contributing to energy-dissipation processes that were responsible for plastic deformation at the microscale. An origin of nanocrystallisation was explained in terms of heating in shear bands, free-volume generation, shear strains or ultrahigh strain rates. Schuh and co-workers proved that SBs in a Zr-based metallic glass demonstrated no obvious long-range order [5,14]. This hypothesis was confirmed in a study by Wilde and Rösner [22], who found no crystallisation in SBs of $Al_{88}Y_7Fe_5$ glass at room temperature. Thus, the question of propensity for crystallisation in SBs of BMGs is still open. With different, sometimes contradicting hypotheses about deformation mechanisms of BMGs at the microscale, further studies are required to understand initiation and propagation of SBs in the volume and on the surface of metallic glasses. Structural characterisation of SBs around a deformed region will help us understand the nature of their formation and evolution [23]. This could help link SB propagation with inelastic deformation of BMGs.

As localised shear-band formation is responsible for inelastic deformations in BMGs, this study focus on the characterisation of shear bands as well as their formation and evolution. It provides a new insight related to shear bands in Zr-Cu-based metallic glass and its deformation under homogeneous (uniaxial compression) and inhomogeneous (wedge indentation) loading conditions. To achieve this, individual SBs were characterised with TEM. Nano- and wedge indentations were carried out to analyse the evolution of SBs through the volume of the BMG employing a surface-decoration technique.

2 Material and Experimental Procedure

A BMG with a nominal composition of $Zr_{48}Cu_{36}Al_8Ag_8$ (at.%) was selected for this study. The alloy was produced at IFW Dresden, Institute for Complex Materials, Germany. The supplied samples were cut using wire electric discharge machining (EDM) into rectangular specimens of approximately 40 mm×2 mm×2 mm for a three-point bending test and 40 mm×5 mm×2 mm for wedge indentation experiments. All samples were polished to mirror finish before experimentation. Structure of the studied alloy was inspected with X-ray diffraction (XRD) using a Rigaku Ultima-III diffractometer with Cu-Kα radiation. The scans were carried out over several locations on the samples that were characterised with TEM (JEM-2000FX, JEOL Ltd, Tokyo, Japan) before and after deformation. For TEM analysis, the samples were thinned to electron transparency using a focussed ion beam system (FIB, FEI Company, Hillsboro, USA). As shown in Fig. 1, only broad amorphous peaks were presented without any indication of crystalline Bragg peaks.The dark field TEM image indicates

that no crystalline phases were found, further confirming the glassy nature of the samples. The halo SAED pattern of the as-cast sample (Fig. 1 b) shows a set of diffuse rings, which is typical of an amorphous structure. The composition of the locations, where the SAED was obtained from, was tested *in-situ* with EDS. The measurement showed that the elemental concentrations were close to the nominal values of the BMG material which is 47.9 at.% Zr, 36.5 at.% Cu, 7.9 at.% Al and 7.7 at.% Ag.

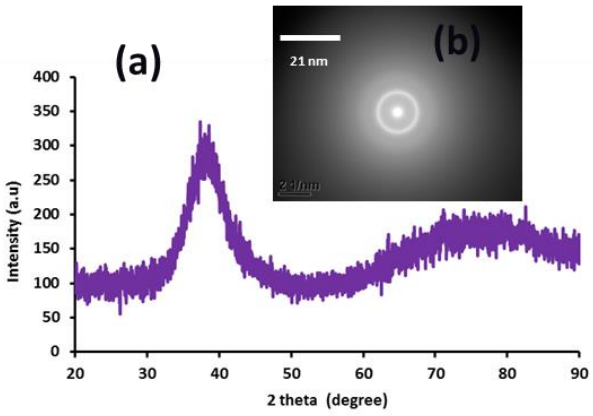

Fig. 1. XRD pattern (a), with corresponding SAED patterns shown in inset (b), of as-cast $Zr_{48}Cu_{36}Al_8Ag_8$

To study SB evolution, interrupted wedge indentation was performed on the BMG component. The wedge indenter was made of high-speed steel (HS 6-5-4), with a wedge angle of 60º and an edge radius of 19.5 µm, designed and manufactured in-house (see Fig. 2). The tests were conducted with an Instron 3345 testing machine, with a displacement rate of 0.5 mm/min. The unloaded samples were analysed with SEM (LEO 1530VP, Carl Zeiss SMT, Germany) on their top and front surfaces (see Fig. 2). First, an initial indentation with a load of 500 N was made on a beam-shaped specimen with dimensions 40 mm×5

mm×2 mm. This was sufficient to initiate shear bands near the point of load application. Next, ten 6×6 sets of grid lines were milled using FIB with 30 kV acceleration voltage and 10 pA beam current on the front surface of the beam. The milled lines had a length of 20 μm, width of 0.2 μm and spacing of 1 μm (Fig. 5). Following this, wedge indentation was performed by loading-unloading at 1 kN and 2 kN. The gridlines were observed with SEM after each unloading step (Fig. 5 a-d).

Subsequently, to characterise the SBs, a series of nano-indentation (Nanotest 600, Micro Materials Wrexham UK) experiments were conducted at and near the SBs (Fig. 9). A fracture surface obtained from conducting a three-point bend test to failure was characterised using a Vickers indenter under peak loads of 500 mN and a loading rate of 2 mN/s with a 30 s hold time at peak load to assess variation in hardness.

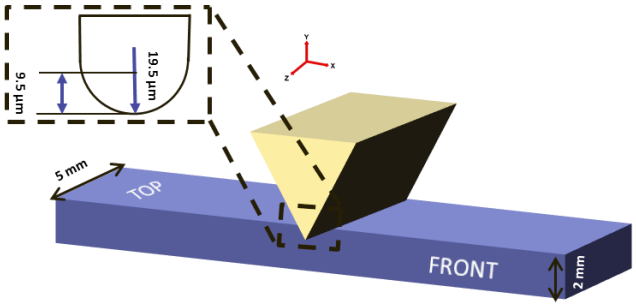

Fig. 2. Schematic of wedge indentation setup for SB observation with wedge dimensions.

Specimens for microcompression studies were prepared from beam-shaped samples of as-cast material and from the fracture surface area (see details in Section 3.3.2). To reduce the effect of a taper, micropillars (see Fig. 3) with a

nominal square cross-sectional area of 10 μm×10 μm and an effective height of 25 μm were prepared with a top-down milling method with FIB by successively reducing the cross-section of the pillar during the milling process. The pillar obtained from the fractured surface was milled to ensure a flat top surface. Ion beam with a 30 kV accelerating voltage was used where an initial current of 20 nA was gradually reduced to 1 nA as the pillar cross section decreased.The tests were performed with a nanoindentation system (MTS nanoindenterXP) using a flat punch tip with an equilateral triangle cross-section with an inside length of 50 μm. All tests were performed at a constant nominal displacement rate of 8 nm/s with a total indenter displacement of 2 μm. The resulting evolution and morphology of microstructure were examined with SEM.

3 Shear-band characterisation

3.1 Shear-band evolution

The surface-decoration technique was used to track formation and evolution of multiple SBs. Shear bands was examined at ten different locations as shown in Fig. 4.

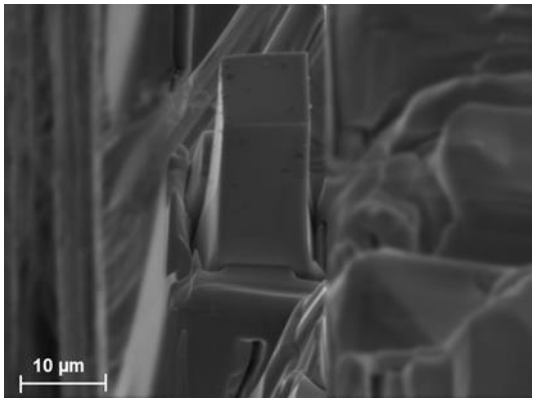

Fig. 3 . Micropillars of as-fabricated $Zr_{48}Cu_{36}Al_8Ag_8$ with a square cross-section of 10 µm×10 µm.

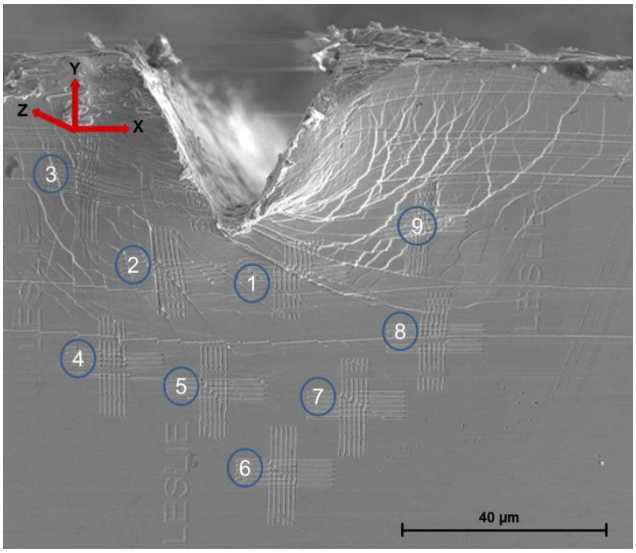

Fig. 4. Surface decoration and locations of areas for SB analysis (numbered from 1 to 9).

It is known that surface imperfections serve as preferred sites for initiation of SBs [25]. We performed several studies to ensure the surface decoration itself do not serve as SB initiation sites. Our studies indicate no obvious differences in SB evolution in specimens with polished and decorated surfaces.

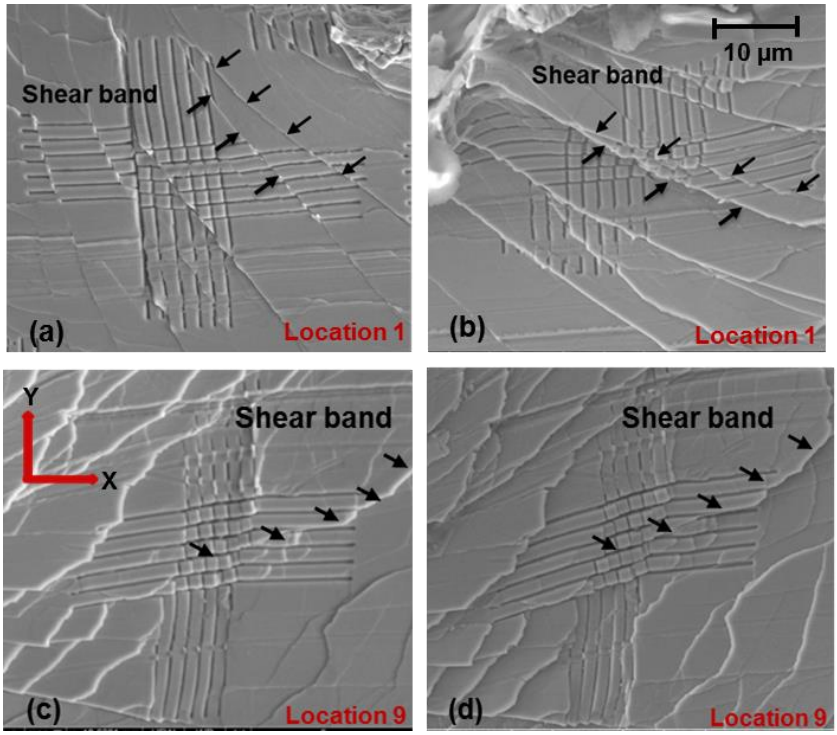

Fig. 5. Evolution of SBs with incremental loading in grid 1 after 1 kN load (a), after 2 kN load (b) and in grid 9 after 1 kN (c) and after 2 kN (d). (Arrows indicate shear band evolution; grids 1 and 9 are shown in Fig. 4.)

As illustrated in Fig. 5, SBs formed a localised deformation zone with slip occurring across these bands as marked by arrows in Fig. 5. This indicates that once an SB was formed, the material volume slipped across it discretely (Fig. 5 b). Our experimental studies show that SBs do not propagate gradually across specimens (no diffusion) associated with SB displacement that occurred in a localised area as proposed by Liu and co-workers [26].

Next, the morphology of the material surface intersected by SBs (front face in Fig. 5 b) was studied using a Zygo NEWVIEW 5000 system. An SB was chosen for this and the variation of height across it was measured at three locations (designated by lines 1, 2 and 3 in Fig. 6 a). The measured profile of the surface

indicates that the variation of height across the SB increases further away from the indenter (Fig. 6 b). Interestingly, depending on location, the material volume seems to have rotated out of plane along the SB. The extent of rotation increased as the SBs propagated out into the bulk material. This was observed across all studied SBs. As an example for the specific shear band analysed in Fig. 6 b, the two surfaces across the SB deviated at a rate of 1.75 (µm/µm). Further studies on this observation are warranted, especially in other BMGs.

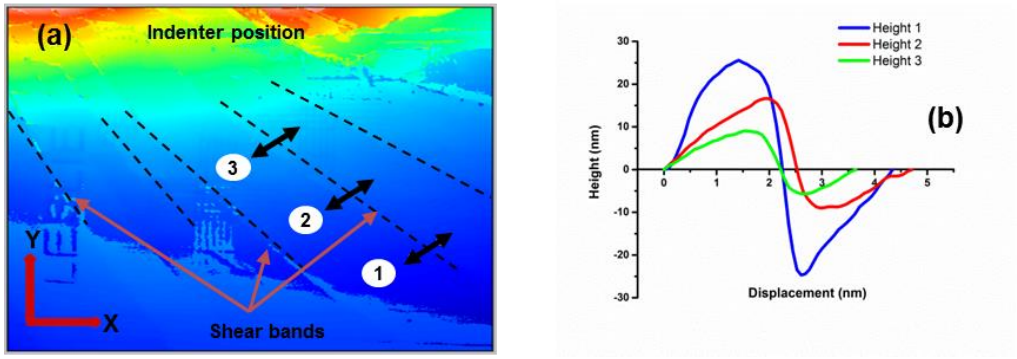

Fig. 6. Measurement of material`s height along single SB: (a) overall appearance of SBs and measurement sites; (b) variation of height along SB for positions shown in (a) (this is a scatter plot with smooth lines)

Evolution of the deformation pattern on the top surface of the indented sample (Fig. 7) provided additional insights into SB formation. The SBs line up along straight lines parallel to the imprint's axis (Fig. 7 b). Contrary to the front surface, no SBs were observed on the top surface at 1 kN (Fig. 7 a). The propagation of SBs was along a hemi-cylindrical path until they reached the sample's top surface, further indicating that nucleation of SBs occur easier than their evolution. Our observations indicate that shear bands were probably initialized in "weak sites", defined by fluctuations of free volume or chemical heterogeneity

of the BMG. Such weak sites control the energy barrier for the operation of SBs. Thus, higher loads are required to activate additional SBs at higher levels of barrier energy to maintain a continuous process of deformation. Once the lower-energy sites are exhausted, the hardening effect levels off and results in a steady-state flow without any significant hardening or softening [15]. At present, given the limitation of the instruments used, these observations are subjective, and a precise quantitative estimate on the ease of SB nucleation compared to their evolution is lacking.

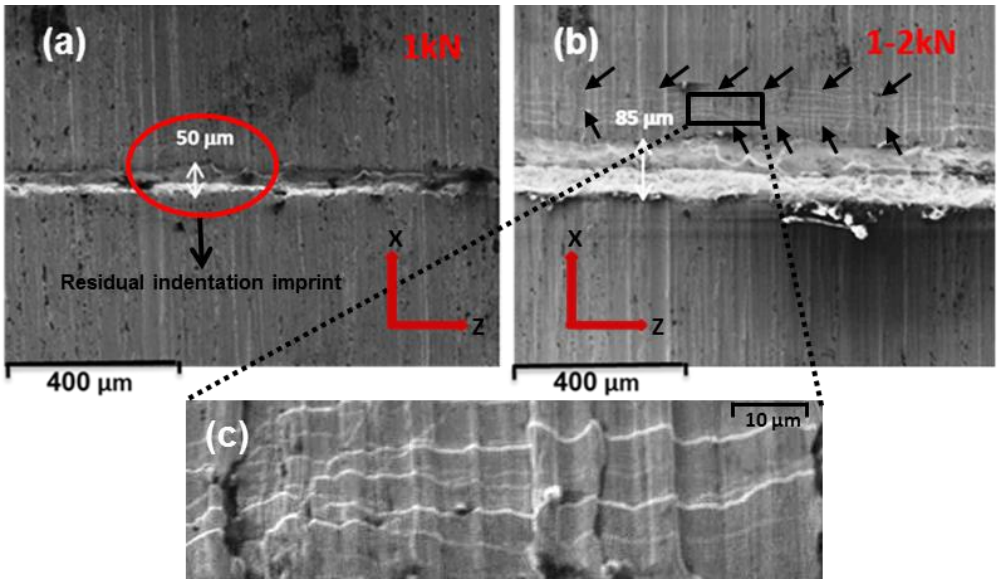

Fig. 7. SEM images of evolution of SBs on top surface with incremental loading under wedge indentation: (a) after imposing 1 kN; (b) after imposing 2 kN; (c) zoom-in of highlighted region in (b). The measured residual imprint width for 1 kN and 2 kN were 50 µm and 85 µm, respectively.

3.2 Microstructural characterisation of shear bands

To assess microstructural characteristic of SBs, TEM studies were performed. Thin-film foils for TEM were prepared using FIB milling. Slices were cut along a

plane parallel to the loading direction and perpendicular to the visible shear planes identified from traces of slip bands on the sample surfaces. In the bright-field image of the cross-section specimens (Fig. 8 b) extracted from a typical location shown in Fig. 8 a, no dark contrast can be seen. Lack of a noticeable contrast between SBs and the surrounding undeformed matrix indicates that there was no significant change in the structure [7,11]. A region within an SB studied by using a 200 nm × 200 nm square selected area aperture demonstrated a diffuse ring (Fig. 8 c) with no sharp diffraction patterns indicating a fully amorphous structure. Observations with high-resolution electron microscopy (HRTEM) further confirm the amorphous nature of the deformed area in Fig. 8 a. In our study, no nano-sized crystallites with a periodic lattice contrast were found (Fig. 8 d). These results are similar to the work by Schuh and co-workers [5], who prove that there was no obvious long-range order for an area beneath the Berkovich indenter in a Zr-based metallic glass. In addition, studies by Greer and co-workers [27] reveal that when nano-crystals were observed in an SB region, at least sometimes they were artefacts of a TEM specimen-preparation technique [14]. This hypothesis was confirmed by Wilde and Rosner, who found no crystallisation in SBs in $Al_{88}Y_7Fe_5$ glass at ambient temperature [22]. However, nanocrystallisation of Ag-rich particles occurred in a $Zr_{48}Cu_{36}Al_8Ag_8$ sample deformed at high temperature due to phase separation as a result of an annealing process [28]. In our study, similar compositions were observed for the as-cast and the deformed BMG using SAED technique; no compositional changes were found in the SB region. Thus, we conclude, deformation in Zr-Cu BMG do not lead to crystallisation.

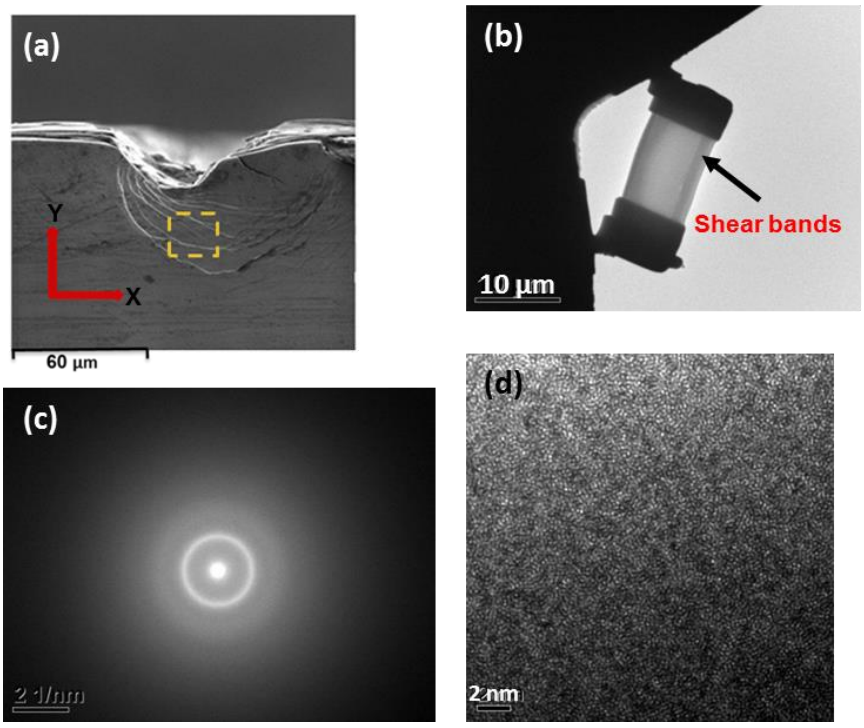

Fig. 8. (a) SEM micrograph of the wedge-indented $Zr_{48}Cu_{36}Al_8Ag_8$ sample with polished surface with traces of SBs. (b) Bright-field TEM image of SBs with dark contrast. (c) Selected area diffraction pattern (d) the representative HRTEM image from deformed region.

3.3 Indentation of shear bands

3.3.1 Individual shear band

As shear band is a unit of plastic deformation in metallic glasses, mechanical properties of individual SBs were investigated in order to obtain a better understanding of the effect of non-crystalline defects on SB induced plasticity. The wedge indentation test was performed with a peak load of 2000 N to obtain well-developed SBs on the front surface of the specimens (see Fig. 2). Under this condition, it is easy to determine the location of SBs in the specimens. Since the indentations were spaced at an interval of 10 µm and the imprint size

was around 5 μm, the spatial resolution perpendicular to the surface and into the SB was within 3 μm. The values of hardness and modulus measured in the deformed region are divided into two groups based on the location of indentation. Indentations made on SBs exhibited higher displacement up to peak-load than those made in the bulk materials (Fig. 10 a), indicating that shear bands were softer.

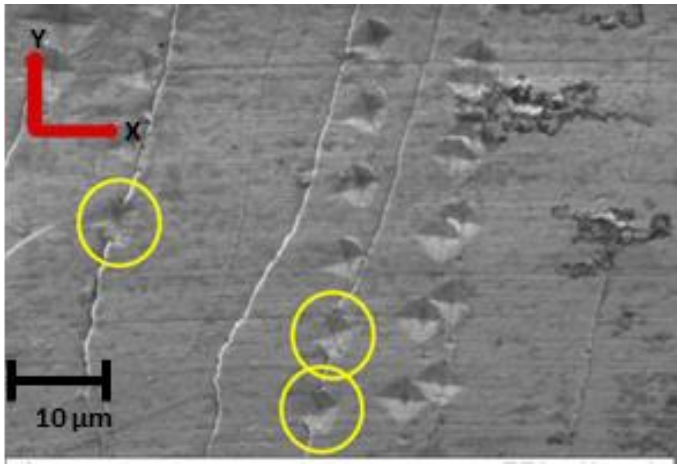

Fig. 9. SEM images of indentations over shear bands and between them.

We note that the indentation on the SB is not in a strict sense representative of the SB properties as the indentation inevitably deforms the surrounding bulk material which is harder. Thus, we expect the SB to be weaker than the hardness value reported via our experiments [29].

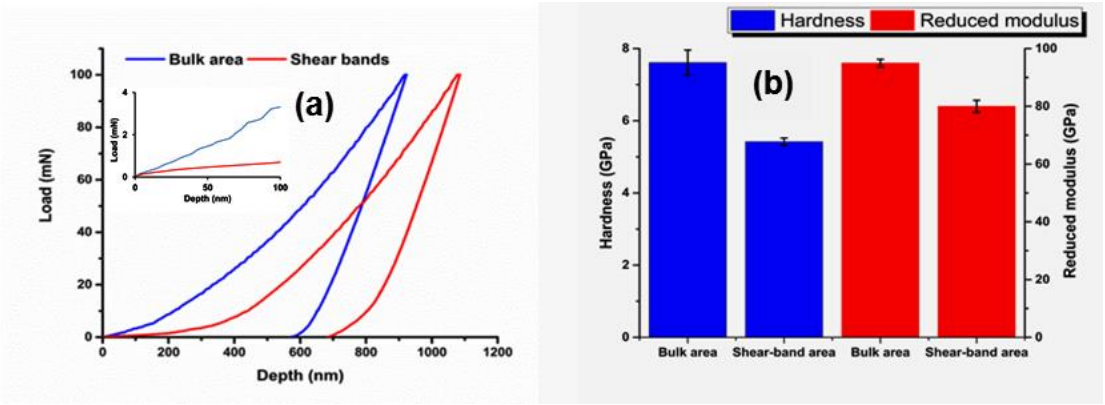

Fig. 10. Comparison of mechanical properties of bulk material and shear-band areas in nanoindentation: (a) load-displacement curve with its initial stage shown in inset (this is a scatter plot with straight lines); (b) hardness and reduced modulus

The sheared zone, which can be considered as an area with multiple SBs, can be estimated from the initial part of the load-indentation depth (P-h) curve shown in Fig. 10 a. As shown in the inset of Fig. 10 a, the load-depth plot demonstrates several serrations, which indicate formation of shear bands [29]. These SBs were uniformly distributed in the sheared region, leading to a combined (akin to a composite) response of shear bands and undeformed region.

3.3.2 Fracture surface

A standard macroscale three-point bending test with an Instron 3345 testing machine was conducted to determine the bulk flexural modulus of the BMG, which was evaluated to be 95 GPa with the Poisson's ratio (ν) of 0.35. This yields a shear modulus (G) of 35 GPa. Simplicity of determining the elastic modulus using the bending test is worth considering in comparison to a tensile

test, which often suffers from fixation, gripping and alignment problems. The sample was tested to failure.

Fracture-surface morphology of the specimen was studied for both tension and compression sites; both showed vein-like structures (Fig. 11 a). Some branches of these structures can be found at the sites where the propagation direction deviated from that of the maximum shear stress. This behaviour is distinctly different from the case of propagation of principal SBs along a slip plane, which was widely reported in the literature [30-32]. As shown in Fig. 11 d, the tension regions of the fracture surface obtained in three-point bending show a classic vein structure of SBs on the surface. Observations of the fracture surface (Fig. 11 a) show localized plastic deformation (demonstrated SB activity) in a zone with a depth of some 10 μm (Fig. 11 b). The zone consisted of several SBs with 10-20 nm thickness. As shown in Fig. 11 c, river patterns were formed as a result of SB sliding. High-magnification images exhibit a micro-scale vein-like pattern in a region of fracture associated with high normal stresses [33]. In contrast to our results, Zhang et al. [34] showed no evident SBs on the fracture surface of $Zr_{48}Cu_{36}Al_8Ag_8$ under pure compressive load.

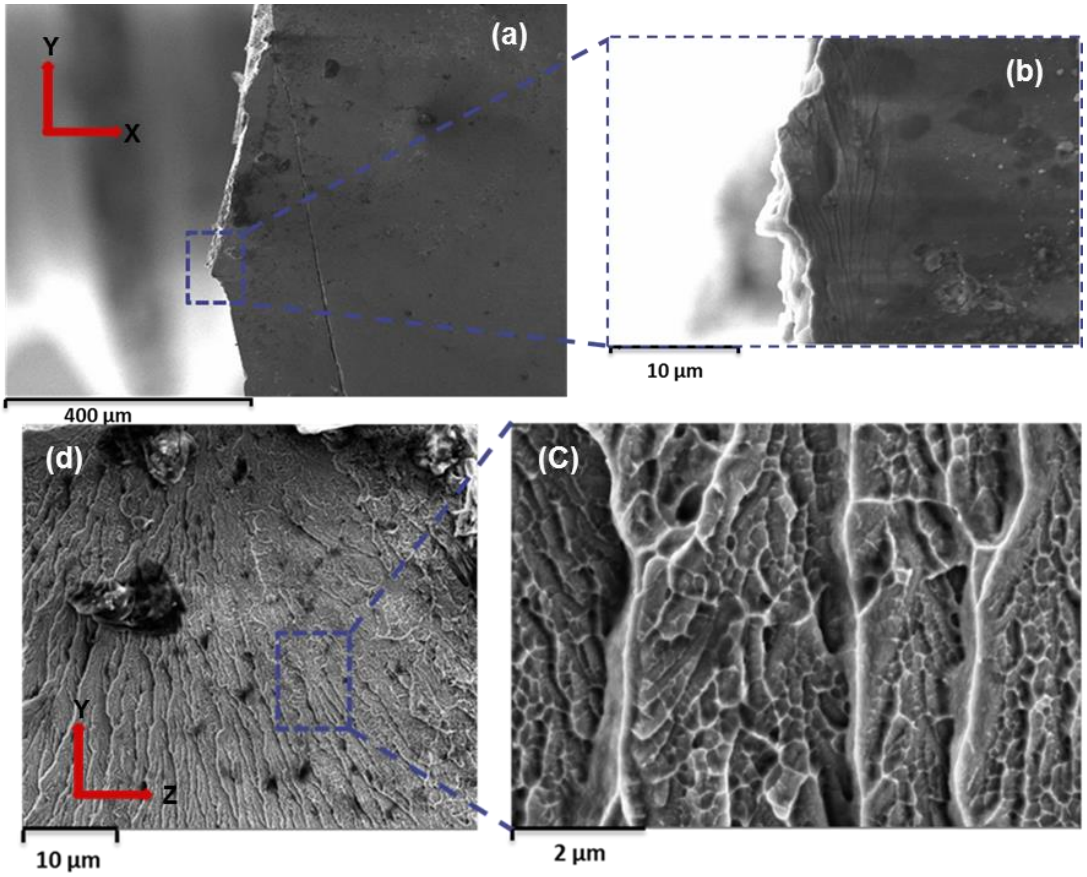

Fig. 11. SEM observations of fracture surface of $Zr_{48}Cu_{36}Al_8Ag_8$ metallic glass failed in three-point bending (a) and multiple shear bands (b) formed in compression associated with SBs. Top view of fracture morphology in tension mode (c) displaying clearly typical vein morphology (d).

Next, nanoindentation tests were carried out on the fracture surfaces of the specimens to assess the effect of the dilatation process, which is considered as a mechanism of deformation-induced localisation. We observe a distinct difference between mechanical properties of the fractured region and of the undeformed material in indentation with 500 mN (Fig. 12). Nominal hardness and modulus of the fracture surface were much lower, with values of 0.5 GPa ($G = 0.19$ GPa) and 20 GPa ($G = 7.4$ GPa) when compared to that of the virgin

material with values of 8 GPa ($G = 3$ GPa) and 90 GPa ($G = 33.5$ GPa), respectively (Fig. 12 a-b). Observed scatter in experimental data may be due to: (1) natural roughness of the fracture surface, affecting the contact area, and/or (2) presence of mechanically softer shear bands. A relatively high load (500 mN) was chosen to ensure that surface asperities do not affect the observed results. Therefore, these results indicate that there are a large number of SBs were activated during the fracture process.

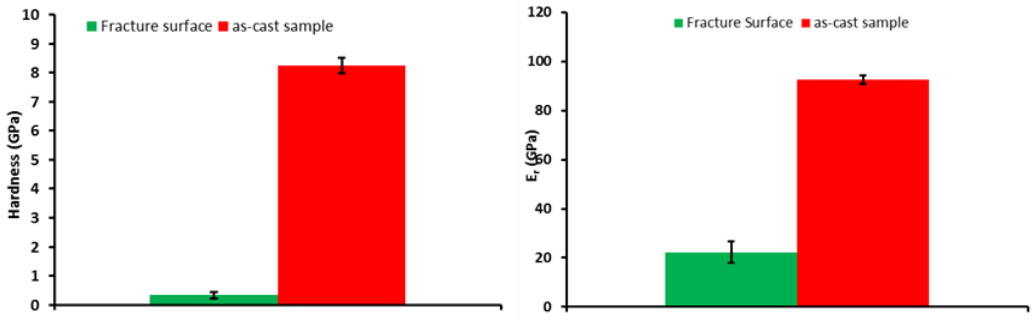

Fig. 12 Fracture surface vs. as-cast sample: (a) hardness; (b) modulus under peak load of 500 mN

To confirm that the lower levels of hardness and the modulus of the fracture surface were not experimental artefacts, nano-indentation experiments were conducted on the specimen's top surface (this surface is approximately orthogonal to the fracture surface) close to the fractured edge. Additional indents were made near the fracture edge within the distance from ~16 μm to 700 μm (Fig. 13) to investigate the variability of mechanical properties in the deformed region. The study demonstrated that the measured modulus varied from ~17 GPa to ~90 GPa (with the latter corresponding to the respective value in the as-cast BMG) depending on the distance to the fracture surface (Fig. 13

b). The measured modulus gradually increased up to ~40 GPa in the region spanning around 400 µm from the fracture surface, followed by a sharp increase to the as-cast level. These results indicated that there was a softened zone, as discussed in the previous section, with a width of ~400 µm followed by a distinct transition from the deformed region to the virgin-state area.

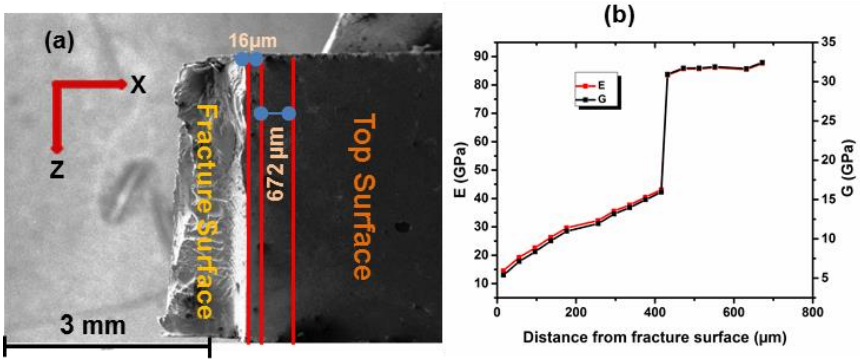

Fig. 13. (a) sample used in experiments illustrating indentation points on fracture surface within the distance from ~16 µm to ~700 µm; (b) variation in measured elastic and shear moduli with distance from fracture surface (the line fit is drawn for visual aid).

As discussed by Meng and co-workers [36], HPT-deformed sample of $Zr_{50}Cu_{40}Al_{10}$ using constrained-geometry anvils under a compressive pressure at room temperature shows a lower modulus and hardness which is similar to the observations made on the fracture surface in unconstrained 3-point bending experiments in our studies.

The onset of serration during the deformation process was probably controlled by the creation and annihilation of free volume leading to the formation of SBs; obviously, experiments could not provide direct evidence of this activity.

However, a number of mechanistic theories were proposed to justify the existence of free volume and shear transformation zones (STZs) [5]. Pre-existing SBs act as preferred sites for further deformation with free volume being potentially increased in the deformed regions. This can lead to formation of a sheared zone contributing to plastic deformation. The sheared zone can be enlarged by nucleation of new shear bands, resulting in enhancing intrinsically the extent of ductility and free-volume creation. Yavari et al. [46] claim that the free volume in deformed metallic-glass ribbons was double that in an as-cast state. Our experimental results were confirmed by Ketov et al. [37] who report a huge reduction of elastic modulus measured using Quantitative Nanomechanical Measurements (QNM) of a Cu-Zr BMG when assessed near single shear bands.

3.4 Microcompression studies

Compression tests were carried out on micropillars milled from the as-cast and fractured surfaces. The morphologies of shear bands in the pillars after compression are shown in Fig. 14. The deformation mode of these pillars was dominated by localised shear banding. As shown in Fig. 14, a concentration of shear bands was observed at the corner of the pillar, indicating minor misalignment in contact of the flat punch (this is marked in the stress-strain plot in Fig. 15) with the pillar surface at the initial stage of deformation [38]. In compression, the upper part of the specimens began to slip along a major shear plane, resulting in the formation of lips on the top of the deformed samples (Fig. 14 (a)). An engineering stress-strain curve comparing the pillars obtained from the two locations is shown in Fig. 15. In the virgin sample, at a stress of ~1.8

GPa a noticeable change in deformation characteristics was observed; it corresponds to the yield strength reported for Zr-Cu-based metallic glass under compression [34]. The elastic modulus was 85 GPa or $G = 31.5$ GPa (after ignoring the initial non-linear stress-strain stemming from contact anomalies and adding a correction factor obtained from finite-element simulations of microcompression accounting for the pillar's boundary effects [39]), which is similar to the result obtained from the three-point bending tests. The pillar from the fractured surface showed a significantly lower elastic modulus (~30 GPa) or $G = 11$ GPa and yield (~1 GPa) (the measured elastic modulus was estimated from the elastic region of an engineering stress-strain curve). This demonstrate that the deformed area was twice softer compared to the as-cast material, which was also confirmed by the indentation tests performed on the fracture surface. The difference in the strength levels is associated with the flaw sensitivity [13] of defect population that helped shear-band initiation [30, 44].

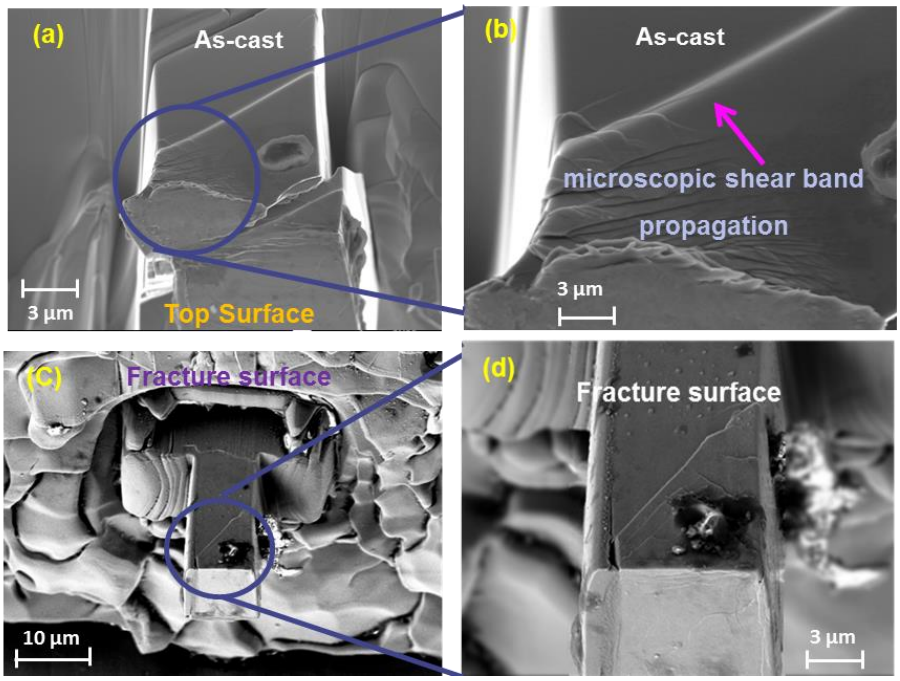

Fig. 14. SEM micrographs of deformed micropillars: (a-b) as-cast micropillar; (c-d) fracture surface.

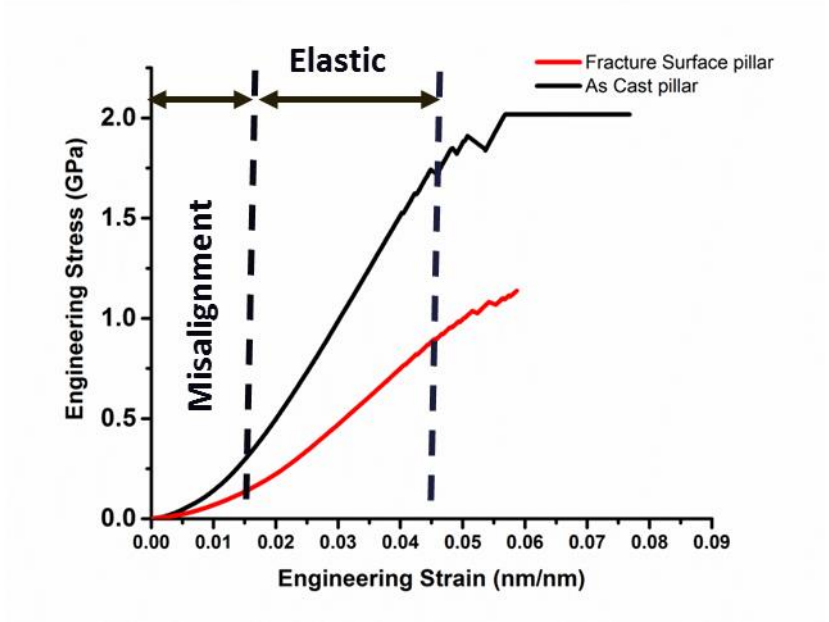

Fig. 15 Microcompression engineering stress-strain curves showing different stages of experiments including misalignment (due to contact anomalies) and linear elasticity with micropillars from virgin (as cast) and shear-zone areas of

$Zr_{48}Cu_{36}Al_8Ag_8$ at constant displacement rate of 8 nm/s (the graph is a scatter plot with straight lines)

4 Concluding Remarks

A systematic study was carried out to investigate features of plastic deformation related to shear bands in $Zr_{48}Cu_{36}Al_8Ag_8$ metallic glass. This analysis provided a new insight into the deformation behaviour of Zr-Cu-based BMGs, and its main conclusions are summarised as follows:

1. During plastic deformation, shear bands formed localised deformation zones, with deformation inducing discrete movement of the material's volume along shear-bands.
2. Our experiments indicate that shear bands would typically form within the material volume before propagating to the surface.
3. Electron microscopy characterisation of individual shear bands revealed that there was no precipitation of nanocrystals inside the shear bands induced by deformation, and that shear bands were amorphous.
4. The fracture surfaces were consisting of multiple localised shear bands and the surface is mechanically proved to ~4 times weaker considering the elastic modulus and ~16 times weaker in hardness than the undeformed material.
5. A mechanically soft zone corresponding to ~400 μm form at the fracture surface which is expected to contain higher volume fraction of free volume.

These experimental observations can form the basis for the development of phenomenological constitutive modelling of BMGs accounting for the non-local nature of plastic deformation in the material.

Acknowledgement

The authors acknowledge the use of facilities of the Loughborough Materials Characterisation Centre (LMCC) at Loughborough University, The UK.

5 References

1. P. Gargarella, S. Pauly, M. Stoica, G. Vaughan , C. Afonso, U. Kühn, J. Eckert, Structural evolution in Ti-Cu-Ni metallic glasses during heating. APL Mater. 3 (2015) 016101.

2. M.K. Dambatta, J. Izman, C. Yahaya, J.Y. Lim, D. Kurniawan, Mg-based bulk metallic glasses for biodegradable impant materials: A review on glass forming ability, mechanical proiperties, and biocompatibility. J. Non-Crys. Solids. 426 (2015) 110-115.

3. M.K. He, S.H. Chen, P.Yu, L. Xia, Enhanced mechanical properties of $Ni_{62}Nb_{38}$ bulk metallic glasses by Ta substitution. J.Non-Crys. Solids. 471 (2017) 452-455.

4. W. Chen, Z. Liu, J. Ketkaew, R.M.O. Mota, S. Kim, M. Power, W. Samela, J. Schroers, Flaw tolerance of metallic glasses. Acta Mater. 107 (2016) 220-228.

5. C.A. Schuh, T.C. Hufnagel, U. Ramamurty, Mechanical behavior of amorphous alloys, Acta Mater. 55 (2007) 4067-4109.

6. M. Chen, Mechanical behavior of metallic glasses: Microscopic understanding of strength and ductility, Annu. Rev. Mater. Res. 38 (2008) 445-469.

7. K. Wang, T. Fujita, Y.Q. Zeng, N. Nishiyama, A. Inoue, M.W. Chen, Micromechanisms of serrated flow in a Ni_{50} Pd_{30} P_{20} bulk metallic glass with a large compression plasticity, Acta Mater. 56 (2008) 2834-2842.

8. T.C. Hufnagel, C.A. Schuh, M.L. Falk, Deformation of metallic glasses: Recent developments in theory, simulations, and experiments. Acta Mater. 109 (2016) 375-393.

9. Y. Zhang, A. Greer, Thickness of shear bands in metallic glasses, Appl. Phys. Lett. 89 (2006) 071907.

10. V. Schmidt, H. Rösner, M. Peterlechner, G. Wilde, P.M. Voyles, Quantitative measurement of density in a shear band of metallic glass monitored along its propagation direction. Phys. Rev. Lett. 115 (2015) 035501.

11. M. Chen, A. Inoue, W. Zhang, T.Sakurai, Extraordinary plasticity of ductile bulk metallic glasses, Phys. Rev. Lett. 96 (2006) 245502.

12. D.C. Hofmann, J. Suh, A. Wiest, G. Duan, M. Lind, M.D. Demetriou, W.L. Johnson, Designing metallic glass matrix composites with high toughness and tensile ductility, Nature 451 (2008) 1085-1089.

13. W. Wu, Y. Li, C.A. Schuh. Strength, plasticity and brittleness of bulk metallic glasses under compression: statistical and geometric effects. Philos. Mag. 88 (2008) 71-89.

14. A.L. Greer, Y.Q. Cheng, E. Ma, Shear bands in metallic glasses, Mater. Sci. Eng. Report 74 (2013) 71-132.

15. Y.H. Liu, C.T Liu, A. Gali, A. Inoue, M.W. Chen, Evolution of shear bands and its correlation with mechanical response of a ductile $Zr_{55}Pd_{10}Cu_{20}Ni_5Al_{10}$ bulk metallic glass, Intermetal. 18 (2010) 1455-1464.

16. Y.M. Chen, T. Ohkubo, T. Mukai, K. Hono, Structure of shear bands in $Pd_{40}Ni_{40}P_{20}$ bulk metallic glass, J. Mater. Res. 24 (2009) 1-9.

17. L. Gu, L. Xu, Q. Zhang, D. Pan, N. Chen, D.V. Louzguine-Luzgin, Direct in situ observation of metallic glass deformation by real-time nano-scale indentation, Sci. Reports 5 (2015) 9122.

18. H. Kimura, T. Masumoto, A model of the mechanics of serrated flow in an amorphous alloy, Acta Metal. Mater. 31 (1983) 231-240.

19. J.Y. Lee, K.H. Han, J.M. Park, K. Chattopadhyay, W.T. Kim, D.H. Kim, Deformation and evolution of shear bands under compressive loading in bulk metallic glasses, Acta Mater. 54 (2006) 5271-5279.

20. M. Jiang, Z. Ling, J. Meng, L. Dai, Energy dissipation in fracture of bulk metallic glasses via inherent competition between local softening and quasi-cleavage. Philos. Mag. 88(2008) 407-426.

21. J.J. Kim, Y. Choi, S. Suresh, A.S. Argon, Nanocrystallization during nanoindentation of a bulk amorphous metal alloy at room temperature, Science 295 (2002) 654-657.

22. H. Rösner, M. Peterlechner, C. Kübel, V. Schmidt, G. Wilde, Density changes in shear bands of a metallic glass determined by correlative analytical transmission electron microscopy, Ultramicroscopy 142 (2014) 1-9.

23. S. Vincent, B.S. Murty, M.J. Kramer, J. Bhatt, Micro and nano indentation studies on $Zr_{60}Cu_{10}Al_{15}Ni_{15}$ bulk metallic glass, Mater. Des. 65 (2015) 98-103.

24. B. Winiarski, G.S. Schajer, P.J. Withers, Surface decoration for improving the accuracy of displacement measurements by digital image correlation in SEM, Exp. Mech. 52 (2012) 793-804.

25. H. Li, A. Ghosh, Y.H. Han, R.C. Bradt, The frictional component of the indentation size effect in low load microhardness testing, J. Mater. Res. 8 (1993) 1028-1032.

26. Z. Liu, R. Wang, R. Qu, Z. Zhang, Precisely predicting and designing the elasticity of metallic glasses, J. Appl. Phys. 115 (2014) 203513.

27. J.R. Greer, J.T.M. De Hosson, Plasticity in small-sized metallic systems: Intrinsic versus extrinsic size effect, Prog. Mater. Sci. 56 (2011) 654-724.

28. D.V. Louzguine-Luzgin, T. Wada, H. Kato, J. Perepezko, A. Inoue, In situ phase separation and flow behavior in the glass transition region. Intermetal. 18 (2010) 1235-1239.

29. J. Pan, Q. Chen, L. Liu, Y. Li, Softening and dilatation in a single shear band, Acta Mater. 59 (2011) 5146-5158.

30. B.E. Schuster, B. Wei, M.H. Ervin, S. Hruszkewycz, M.K. Miller, T.C. Hufnagel, Bulk and microscale compressive properties of Pd-based metallic glass, Scr. Mater. 57 (2007) 517-520.

31. T.C. Hufnagel, P. El-Deiry, R. Vinci, Development of shear band structure during deformation of a $Zr_{57}Ti_5Cu_{20}Ni_8Al_{10}$ bulk metallic glass, Scr. Mater. 43 (2000) 1071-1075.

32. H. Bei, S. Xie, E.P. George, Softening caused by profuse shear banding in a bulk metallic glass, Phys. Rev. Lett. 96 (2006) 105503.

33. A. Inoue, T. Zhang, T. Masumoto, Glass-forming ability of alloys, J. Non-Cryst. Solids 156–158 (1993) 473-480.

34. Q. Zhang, W. Zhang, G. Xie, A. Inoue, Synthesis, structure and mechanical properties of Zr-Cu-based bulk metallic glass composites. Int. J. Min. Metal. Mater. 17(2010) 208-213.

35. Y. Liu, C.T. Liu, W. Wang, A. Inoue, T. Sakurai, M. Chen, Thermodynamic origins of shear band formation and the universal scaling law of metallic glass strength. Phys. Rev. Lett. 103 (2008) 065504.

36. F. Meng, K. Tsuchiya, I. Seiichiro, Y. Yokoyama, Reversible transition of deformation mode by structural rejuvenation and relaxation in bulk metallic glass. Appl. Phys. Lett. 101 (2012) 121914.

37. S. Ketov, H. Nguyen, A. Trifonov, K. Nakajima, D. Louzguine-Luzgin, Huge reduction of Young's modulus near a shear band in metallic glass. J. Alloys. Comp. 687 (2016) 221-226.

38. C.J. Lee, J.C. Huang, T.G. Nieh, Sample size effect and microcompression of $Mg_{65}Cu_{25}Gd_{10}$ metallic glass, Appl. Phys. Lett. 91 (2007) 161913-162100.

39. H. Zhang, B.E. WU, Q. Wei, K.T. Ramesh, The design of accurate micro-compression experiments, Scr. Mater. 54 (2006) 181-186.

40. W. Weibull, Wide applicability, J. Appl. Mech 33 (1951) 103.

41. Z.P. Bazant, M.Jirasek, Nonlocal integral formulation of plasticity and damage: Survay of progress, J. Eng. Mec. 128 (2002) 1119-1149

42 R.H.J. Peerling, M.G.D. Geers, R. de Borst, W.A.M. Brekelmans, A critical comparison of nonlocal and gradient-enhanced softening continua, Int. J. Solids. Struct. 38 (2001) 7723-7746.

43. P.A. Vermeer, B.J. Brinkgreve, Localisation and Bifurcation Theory for Soils and Rock 23 (1994) 89-100.

44. C. Volkert, A. Donohue, A. Spaepen, Effect of sample size on deformation in amorphous metals, J. Appl. Phys 103 (2008) 3539.

45. V. Nekouie, A. Roy, V.V. Silberschmidt, Indentation study of mechanical behaviour of Zr-Cu-based metallic glass, IPME (2015) 291-299.

47. A.R. Yavari, A.L. Moulec, A. Inoue, N. Nishiyama, N. Lupu, E. Matsubara, Excess free volume in metallic glasses measured by X-ray diffraction, Acta Mater. 53 (2005) 1611-1619.